

Urban emission hot spots as sources for remote aerosol deposition

D. Kunkel,¹ M. G. Lawrence,^{1,2} H. Tost,³ A. Kerckweg,³ P. Jöckel,⁴ and S. Borrmann^{1,3}

Received 4 October 2011; revised 2 December 2011; accepted 8 December 2011; published 14 January 2012.

[1] Large point sources such as major population centers (MPCs) emit pollutants which can be deposited nearby or transported over long distances before deposition. We have used tracer simulations of aerosols emitted from MPCs worldwide to assess the fractions which are deposited at various distances away from their source location. Considering only source location, prevailing meteorology, and the aerosol size and solubility, we show that fine aerosol particles have a high potential to pollute remote regions. About half of the emitted mass of aerosol tracers with an ambient diameter $\leq 1.0 \mu\text{m}$ is typically deposited in regions more than 1000 km away from the source. Furthermore, using the Köppen-Geiger climate classification to categorize the sources into various climate classes we find substantial differences in the deposition potential between these classes. Tracers originating in arid regions show the largest remote deposition potentials, with values more than doubled compared to the smallest potentials from tracers in tropical regions. Seasonal changes in atmospheric conditions lead to variations in the remote deposition potentials. On average the remote deposition potentials in summer correspond to about 70–80% of the values in winter, with a large spread among the climate classes. For tracers from tropical regions the summer remote deposition values are only about 31% of the winter values, while they are about 95% for tracers from arid regions. **Citation:** Kunkel, D., M. G. Lawrence, H. Tost, A. Kerckweg, P. Jöckel, and S. Borrmann (2012), Urban emission hot spots as sources for remote aerosol deposition, *Geophys. Res. Lett.*, 39, L01808, doi:10.1029/2011GL049634.

1. Introduction

[2] Major population centers (MPCs) represent an agglomerate of localized emissions with a small spatial appearance on the global scale, but a footprint of great research interest [e.g., Guttikunda *et al.*, 2003; Lawrence *et al.*, 2007; Butler and Lawrence, 2009; Emmons *et al.*, 2010]. Air quality regulations in large cities aim to decrease the pollution level in the cities while grappling with contributions of pollutants from surrounding areas [e.g., Streets *et al.*, 2007; Baklanov *et al.*, 2009; Wang *et al.*, 2010]. Anthropogenic activities like biomass, biofuel, and fossil fuel combustion add trace gases and aerosol particles in large quantities to the atmosphere and consequently perturb the background conditions.

[3] Aerosol particles emitted from MPCs are of great interest due to the consequences they are associated with, for instance to alter earth's radiative budget or their large direct impact on humans, animals, and vegetation when they are close to the surface, which is the case in regions of emission and deposition [e.g., Pöschl, 2005]. Tropospheric aerosol particles often consist of various chemical compounds, depending on their source. Their composition and size strongly determine in which transformation processes they are involved in the atmosphere. Whether an aerosol particle is activated as a cloud condensation nucleus is directly associated with its hygroscopicity or its ability to take up water and grow [Pöschl, 2005]. Activated aerosol particles are subsequently removed more efficiently from the atmosphere via precipitation and thus the residence time in the atmosphere decreases. Shorter residence times commonly coincide with shorter travel distances in the atmosphere. Another limiting factor for travel in the atmosphere is the size of the aerosol particle: the larger it is, the faster it is normally removed by sedimentation from the atmosphere. Nevertheless, measurements have shown that even large aerosol particles, e.g. Saharan dust, can travel long distances [e.g., Betzer *et al.*, 1988]. Wagstrom and Pandis [2010] showed that aerosol particles can experience long-range transport on continental scales, while e.g., Liu *et al.* [2009] showed that different kinds of aerosols can experience inter-continental transport and decrease air quality at the surface and in the free troposphere several thousands of kilometers away from their source.

[4] An important question which arises from these studies is: what fraction of aerosol particles emitted from MPCs is transported to various distances away from their source before being deposited, and how does this depend on the location of the MPC and the aerosol characteristics? To our knowledge, this question has not been addressed in previous studies, which have instead either focused on specific transport events, or on generic gas phase tracers with various atmospheric lifetimes [e.g., Stohl *et al.*, 2002; Lawrence *et al.*, 2007] or precursor gases to determine ozone levels [e.g., Jaffe *et al.*, 1999; Wild and Akimoto, 2001]. Here we apply a global atmospheric chemistry general circulation model (AC-GCM) to address this question, examining the dispersion, general deposition patterns, and remote deposition fractions of artificial aerosol tracers, which all have the same emission source strength from a large set of MPC sources distributed around the world.

2. Model and Experiments

[5] This study extends on that of Lawrence *et al.* [2007] using a different model with aerosol rather than gas phase tracers. We use a set of 46 major population centers worldwide (see Table S1 in Text S1 in the auxiliary material) as emission sources to study the dispersion and deposition of generic aerosol tracers with the global AC-GCM EMAC [Jöckel *et al.*,

¹Max Planck Institute for Chemistry, Mainz, Germany.

²Now at Institute for Advanced Sustainability Studies, Potsdam, Germany.

³Institute for Atmospheric Physics, Johannes-Gutenberg University, Mainz, Germany.

⁴Deutsches Zentrum für Luft und Raumfahrt, Institut für Physik der Atmosphäre, Oberpfaffenhofen, Germany.

2006].¹ The model includes the Modular Earth Submodel System (MESSy, version 1.9, www.messy-interface.org) [Jöckel *et al.*, 2005] which allows the inclusion of different submodels for physical and chemical processes in the atmosphere and interactions between the atmosphere and biosphere. MESSy is coupled to the general circulation model ECHAM5 (version 5.3.01) [Roeckner *et al.*, 2006] which calculates spatial and temporal distributions of atmospheric and surface variables. The model provides a good representation of gas phase tracers [e.g., Jöckel *et al.*, 2006; Tost *et al.*, 2007] and aerosols [e.g., Pringle *et al.*, 2010] in the atmosphere. EMAC has been used for several aerosol tracer studies, e.g., Burrows *et al.* [2009] used generic aerosol tracers to determine the transport of bacteria between different ecosystems and Lelieveld *et al.* [2011] used a similar approach to assess the risk of contamination from radioactive fallout of Cesium-137 after a major nuclear accident.

[6] The applied spectral resolution of the ECHAM5 base model is T106, which corresponds to a horizontal resolution of the quadratic Gaussian grid of about 1.125° in longitude and latitude with 31 hybrid sigma levels in the vertical from the surface up to 10hPa. The model was applied for 18 months, starting in July 2004 with the first six months being used for model spin-up. The year 2005 was chosen for analysis as it is a neutral year in terms of ENSO and coincides with the base year within the MEGAPOLI project [Baklanov *et al.*, 2009]. The meteorological variables vorticity, divergence, logarithm of surface pressure, and temperature are nudged with analysis data from the ECMWF ERA-INTERIM project [Dee *et al.*, 2011] in the course of the simulation.

[7] Our model setup consists of emission, tracer transport, and deposition. The emission is set to be constant in time for each grid box hosting an MPC source point. These grid boxes are located in the lowest model layer and have a mean depth of about 60 m and a horizontal extent of about 100 km. Pozzer *et al.* [2009] discussed the impact of the vertical distribution of trace gas emissions on tropospheric chemistry and found that substantial deviations can occur close to the source but the overall effect on the chemical composition is rather low. Nevertheless, emissions from sufficiently high stacks might be directly released in the atmosphere above the planetary boundary layer and thus increase the potential transport distance. Neglecting such elevated emissions, we obtain a conservative estimate for our long-range transport results. The generic aerosol tracers undergo atmospheric transport with no chemical or micro-physical transformation. Transport of mixing ratios in the model includes horizontal advection [Lin and Rood, 1996], convection [Tiedtke, 1989; Tost *et al.*, 2010], vertical diffusion by turbulent mixing [Roeckner *et al.*, 2006], and gravitational settling [Kerckweg *et al.*, 2006]. Removal of aerosols is calculated by four independent processes: 1) aerosol sedimentation onto the surface, 2) dry deposition by contact with the surface based on its roughness and the boundary layer mixing [Kerckweg *et al.*, 2006], and 3) nucleation and 4) impaction scavenging leading to wet removal in convective and large-scale clouds [Tost *et al.*, 2006]. In the following we refer to dry removal as the sum of sedimentation and dry deposition and to wet removal as the sum of nucleation and impaction

scavenging. More information about the applied submodels can be found in Table S2 in Text S1.

[8] Mono-modal aerosols with ambient diameters of 0.1, 0.5, 1.0, 2.5, and $10.0 \mu\text{m}$ and fix standard deviation of 1.0 are used for two aerosol pseudo-activation regimes. The different aerosol tracer sizes do not interact but provide information on the various parts of the aerosol size distribution. Detailed aerosol chemistry is computationally expensive on global scale for such a large number of source points. Thus, two aerosol solubility states are computed leading to a different treatment within the size-dependent nucleation scavenging:

[9] 1. NS_{act} tracers: all aerosol tracers can undergo nucleation scavenging and show a shorter atmospheric residence time due to stronger rain-out and thus represent a lower limit of the results with respect to the nucleation scavenging activation state;

[10] 2. NS_{inact} tracers: nucleation scavenging is completely inhibited due to the insolubility of the particles representing an upper limit of the results.

[11] The range of sizes and nucleation scavenging activation used here make the results representative for most of the range of real atmospheric aerosol particles.

[12] The global aerosol residence time in the atmosphere varies from less than a day for some of the $10.0 \mu\text{m}$ sized aerosol tracers up to two weeks for small tracers (here defined as particles with ambient diameter $\leq 1.0 \mu\text{m}$). The small aerosol tracers can be interpreted as primary solid aerosol particles like black carbon or soluble secondary organic or inorganic particles. The aerosol tracers with a diameter of $2.5 \mu\text{m}$ represent the largest aerosols that are still classified as fine particulate matter used for air quality regulations (compare $\text{PM}_{2.5}$ = aerosol mass of particles with an aerodynamic diameter smaller $2.5 \mu\text{m}$). These aerosols are distinguished from larger particles, here the $10.0 \mu\text{m}$ tracers, which represent fractions of dust, sea-salt, and sometimes minor amounts of organic matter present in urban centers.

[13] Similar to the pollution potentials in work by Lawrence *et al.* [2007], we define a deposition potential of MPCs. We use the same constant emission rate for each of the MPCs to gain overall knowledge about which MPCs have the largest potentials for long-range pollution by only taking into account location and prevailing meteorology at the emission source, along with the aerosol characteristics. The constant emissions for each source point allow us to scale the results by the total emission and focus on relative fractions of total emission rather than absolute values for the interpretation of the results.

3. Results

[14] We find that small aerosol tracers of various sizes all behave very similarly in their dispersion and deposition. Therefore, we concentrate the discussion of global deposition patterns first on two sizes, $1.0 \mu\text{m}$ and $10.0 \mu\text{m}$ ambient diameter. Aerosol tracers with $2.5 \mu\text{m}$ diameter represent a transition toward the $10.0 \mu\text{m}$ aerosol tracer which will be shown afterwards when metrics are defined to describe the remote deposition.

3.1. Global Deposition Patterns

[15] Figure 1a shows yearly averaged total column densities and Figure 1b shows the annual accumulated total

¹Auxiliary materials are available in the HTML. doi:10.1029/2011GL049634.

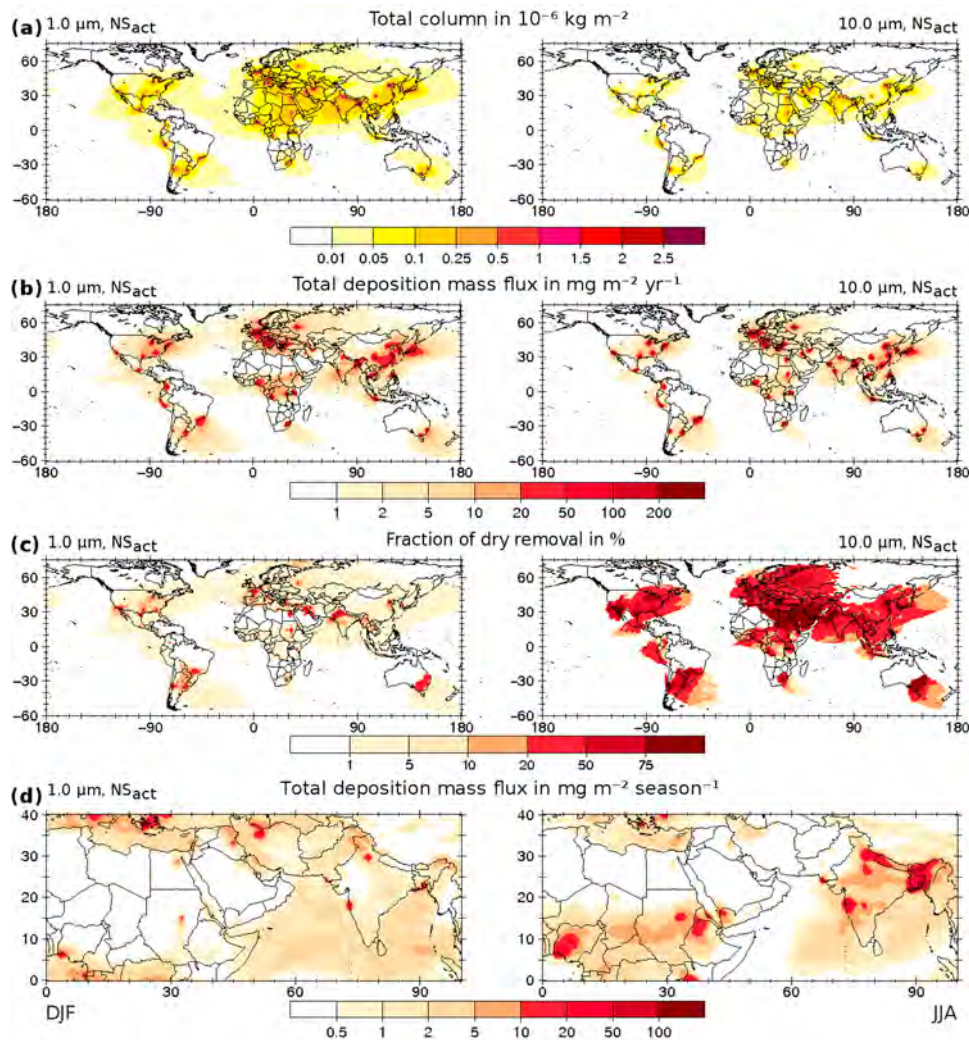


Figure 1. (a) Annual means of total column densities and (b) annual accumulated total deposition mass fluxes for NS_{act} $1.0 \mu\text{m}$ and $10.0 \mu\text{m}$ aerosol tracers. (c) Fractions of dry removed deposition mass fluxes for NS_{act} $1.0 \mu\text{m}$ and $10.0 \mu\text{m}$ aerosol tracers. (d) Seasonally accumulated total deposition mass fluxes for NS_{act} $1.0 \mu\text{m}$ aerosol tracers in boreal winter (DJF) and summer (JJA).

deposition mass fluxes (DMFs) for all 46 major population centers (MPCs). Figure 1 (left) shows distributions for the $1.0 \mu\text{m}$ NS_{act} tracers, and Figure 1 (right) shows distributions for the $10.0 \mu\text{m}$ NS_{act} tracers. Column densities and total DMFs are focused over regions with high concentrations of MPCs, like eastern USA, Europe, South and East Asia, parts of South America and Africa. Maximum values are found near the emission sources, where both dry and wet deposition processes contribute to the total deposition. Aerosol tracers with a diameter of $1.0 \mu\text{m}$ show significant deposition values over large parts of the Atlantic Ocean. In some regions, notable DMFs are seen for tracers with a diameter of $10.0 \mu\text{m}$ where no deposition is evident for tracers with $1.0 \mu\text{m}$ diameter. An example is the Eastern Sahara, which experiences the main southward outflow of the Cairo tracer. The aerosol tracers have to travel through the hot and dry Sahara before they reach the humid region of the Inner-Tropical Convergence Zone (ITCZ), where small aerosol tracers are effectively washed out. In contrast, large aerosol tracers are removed via sedimentation in larger amounts during the

transport through the Sahara due to their higher gravitational settling velocities.

[16] In Figure 1c, the percentage of total DMFs due to dry deposition is shown for both the $1.0 \mu\text{m}$ and $10.0 \mu\text{m}$ NS_{act} tracers. Comparing both sizes a shift in the ratio between dry and wet deposition is observed. Deposition of small tracers mainly occurs via wet removal. On average more than 90% of the total emitted mass is removed by wet deposition, regardless of the nucleation scavenging activation. In contrast, we find that only 38% (NS_{inact}) to 45% (NS_{act}) of the total emissions are wet deposited for $10.0 \mu\text{m}$ tracers. Wet removal of the tracers depends on the presence of clouds and precipitation and can occur in large parts of the troposphere. Dry removal is limited to the lowest model layer and depends on parameters like surface roughness for dry deposition or the mass of the aerosol particle in the case of sedimentation. About 34% of the emissions of large particles sediment onto the ground due to their weight, in contrast to less than 1% for small tracers, both numbers averaged over the nucleation scavenging activation state and for all MPCs. Regions near

Table 1. Annual Mean Remote Deposition Mass Fractions and the Standard Deviations Shown for the Five Aerosol Sizes and Two Nucleation Scavenging Activation Regimes in Regions Outside of Circles With Radii 50, 500, 1000, and 2000 km Around the MPCs

Size	Nucleation Scavenging				
	50 km	500 km	1000 km	2000 km	
0.1	act	89.1 ± 4.8	61.3 ± 11.7	43.6 ± 13.9	23.8 ± 11.7
	inact	92.5 ± 3.3	70.1 ± 9.9	53.9 ± 12.3	33.8 ± 12.3
0.5	act	89.5 ± 4.7	62.0 ± 11.8	44.3 ± 14.1	24.3 ± 11.9
	inact	93.0 ± 3.4	71.0 ± 10.1	55.0 ± 12.6	34.7 ± 12.4
1.0	act	89.4 ± 4.7	61.8 ± 11.8	44.0 ± 14.0	24.1 ± 11.8
	inact	92.8 ± 3.5	70.7 ± 10.1	54.7 ± 12.4	34.4 ± 12.3
2.5	act	87.8 ± 4.7	59.2 ± 11.2	41.8 ± 13.2	22.6 ± 11.0
	inact	91.1 ± 3.6	67.7 ± 9.7	51.8 ± 11.7	32.1 ± 11.5
10.0	act	69.1 ± 6.9	33.7 ± 7.6	20.4 ± 6.9	9.0 ± 4.8
	inact	71.1 ± 7.3	38.0 ± 7.4	24.8 ± 6.7	12.4 ± 4.8

the emission sources show a large aerosol tracer abundance at low levels. Consequently, large aerosol tracers show higher dry DMFs near their source. In turn, small tracers are rapidly vertically mixed or directly lifted into regions with an higher potential for long-range transport. The small tracers are then primarily wet removed in regions farther away from their source points. NS_{inact} tracers have slightly higher dry removal fractions since their wet deposition is reduced. Thus, the characteristics of the deposition potential vary mainly with the aerosol size and also slightly with the activation regime for different regions.

[17] Furthermore, meteorological conditions are responsible for inter-seasonal differences in total DMFs. For the example of Cairo, a local deposition maximum is found during boreal winter (Figure 1d), following the seasonal cycle of precipitation. The influence of precipitation on DMFs is also evident in other regions in Figure 1d. The shift of the African and Southern Asian ITCZ from its southernmost position during DJF to its northernmost position during JJA is clearly marked by the location of the maximum of the DMFs. DMFs over the Indian Peninsula are also strongly affected by the seasonal reversal in the monsoon wind direction, with deposition primarily to the south over the Indian Ocean in DJF and over the continent in the rainiest and most polluted regions (e.g., Western Ghats and Indo-Gangetic Plain) in JJA.

3.2. Remote Deposition

[18] Our main focus in this study is on the fraction of remotely deposited mass, i.e. the mass removed from the atmosphere after traveling for a certain distance through the atmosphere. For this purpose we utilize circles centered at the points of emission. A circle on the surface of the Earth has the shape of an ellipsoid which is based here on the WGS84 ellipsoid [cf. Lawrence *et al.*, 2007]. The maximum deviation of the area of such an ellipsoid is less than 8% from the analytically derived area of a circle with the same radius.

[19] The study's main outcome is presented in Table 1, which lists annually accumulated remote deposition mass fractions and the corresponding standard deviations. The numbers represent averaged values for all 46 tracers, given for four circles with radii of 50, 500, 1000, and 2000 km and for each aerosol diameter and activation state, and give the fraction of the emission which is deposited outside of the corresponding circle. The single emitting grid cells

correspond to a radius of approximately 50 km. The remote deposition fractions for NS_{inact} tracers is always larger than for NS_{act} tracers, justifying the interpretation of the simulations mentioned above as upper and lower bounds of the results. The difference between the two nucleation scavenging activation states generally increases with increasing radius of the circles, except for aerosol tracers with diameter of 10.0 μm , showing almost constant differences. For a given radius of a circle, the small tracers ($\leq 1 \mu\text{m}$) show similar results in their remote deposition mass fractions, while these numbers are smaller and decrease faster for increasing radii for the large aerosol tracers.

[20] The gray shaded area in Figure 2 shows the fractional deposition beyond 1000 km, averaged over all MPCs (with individual lines for averages of various climate classes, see below). For small tracers, on average about 50% of the MPC emissions are deposited in regions more than 1000 km away from the source. Nearly the same result is found for the 2.5 μm aerosol tracers, while the amount deposited beyond 1000 km away is still about 25% for large aerosol tracers.

[21] Furthermore, we categorize the MPCs with help of the Köppen-Geiger climate classification, which is based on temperature and precipitation [Peel *et al.*, 2007]. Hence, we can derive regional differences in the deposition potential for the MPCs taking into account meteorological conditions in the source region. We use six classes: one for tropical regions, i.e. tracers from cities which are classified with A in the climate classification, one for arid regions (class B), one for cold regions (class D), and three for tracers from temperate regions (class C) with dry summer (subclass Cs), dry winter (subclass Cw), or without a dry season (subclass Cf). No MPCs are located in Arctic regions (class E). This

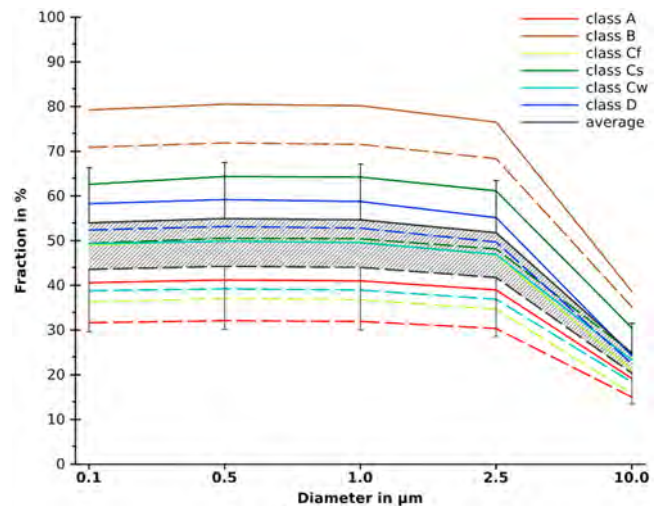


Figure 2. Annual means of the remote deposition mass fraction which is removed outside of a circle centered at the source with a radius of 1000 km. Each line consists of five data points for each size simulated with one standard deviation plotted one-sided. Dashed lines are drawn for NS_{act} tracers, solid lines for NS_{inact} tracers. The gray shaded area represents the overall mean results bounded by the mean results for NS_{inact} tracers at the top and the mean results for NS_{act} tracers at the bottom. Each colored line represents a climate class. No shading is used for climate classes to keep lucidity.

reduces the number of 460 tracers (46 cities \times five sizes \times two NS activation regimes) to 60 values (six classes \times five sizes \times two NS activation regimes). Differences in remote deposition fractions between MPCs in one climate class are always less than 10%, while the differences for the mean values of remote deposition fractions vary strongly between the classes, with the smallest differences for large aerosol tracers in all classes (2.8%–7.5%) and for all tracers in the cold regions (about 3.8%). Small differences in mean remote deposition mass fractions are found for classes Cf and Cw as well as for Cs and D. Between class B and all other classes large differences occur, with a maximum difference between arid (class B) and tropical (class A) classes of about 40%.

[22] This classification of MPCs highlights two points. First, the difference between NS_{inact} and NS_{act} aerosol tracers is rather constant for each climate class, about 10% for small tracers and about 4% for large tracers. Second, it is well known that wet deposition is the dominant removal process for small aerosols. The differing results for the climate classes might suggest that wet removal contributes in different amounts to the overall deposition in each climate class. However, in both cases, for minimal (class A) and for maximal (class B) remote deposition mass fraction, about 95% of the emissions are removed by wet deposition. For a circle with a 1000 km radius, aerosol tracers from arid regions (class B) have a remote deposition mass fraction of about 75%, while for tracers from tropical regions (class A) this is less than half as much (about 36%). This reflects the general difference in the transport distances from source to sink regions for the two classes, with MPCs in arid regions (e.g., Cairo, Teheran, Baghdad) experiencing substantially less wet removal near their source and thus more transport into regions with precipitation farther downwind, while for tracers from tropical regions, the main sink regions are the same as the source regions. Thus, source and sink regions seem to play an important role in characterizing the remote pollution potential for aerosols of the same size.

[23] The remote deposition mass fractions can again be split into their dry and wet removal components. Considering deposition beyond circle of 1000 km radius, dry removal accounts for only 3.8% of the remote deposition mass fraction of the small tracers, while this number increases to about 30% for the large tracers. In fact, no single climate class exceeds a dry remote removal mass fraction of more than 6% for the small tracers. In contrast, maximum values for large tracers amount to about 40% dry remote removal in cold (class D) and temperate regions with dry summer (class Cs) and to about 25% in tropical (class A) and temperate regions with dry winter (class Cw).

[24] Remote deposition mass fractions also show seasonal variations. During winter the range between climate classes is smallest, with generally higher values for the remote deposition mass fractions, while the range is maximum in the summer. Furthermore, the order of the climate classes changes with season. Tracers from tropical and cold regions show rather high remote deposition mass fractions in the winter season, but low fractions in the summer season.

4. Conclusions

[25] We show by means of an aerosol tracer transport study that large amounts of fine particulate matter (ambient diameter $\leq 2.5 \mu\text{m}$) from urban point sources travel long distances

in the atmosphere, with consequent substantial remote deposition. About 50% of the emissions are deposited outside of a circle with a radius of 1000 km which is centered at the emission point for aerosol tracers with ambient diameter $\leq 1.0 \mu\text{m}$ and still 46% for aerosol tracers with ambient diameter of $2.5 \mu\text{m}$. The largest remote deposition potential, e.g., for deposition beyond 1000 km is found for aerosol tracers from MPCs located in arid regions (75%), the lowest for those in tropical regions (36%). The main processes determining the remote deposition mass fractions are the prevailing circulation patterns along with precipitation. Seasonal changes of these meteorological characteristics lead to inter-seasonal variations in the deposition potential of MPCs.

[26] Observations of extreme long-range transport of aerosols from point sources are often associated with pyrogenic convection or volcanic eruptions introducing the emissions at high altitudes into the atmosphere. Our results show that aerosol particles from surface point sources also undergo substantial long-range transport and contribute significantly to remote deposition. For quantitative estimates for specific aerosol species, more detailed emission and micro-physical schemes would have to be applied. Nevertheless, since our tracers cover most of the range of the real aerosol pollutants found in the atmosphere the results can be seen as a clear indication that not only local dwellers profit from air quality regulations for aerosols, but also to a large extent people living hundreds of kilometers downwind of one or several heavily urbanized areas. In particular, if a region is downwind of several MPCs, it might experience cumulative pollution from two or more MPCs as well as an increased frequency of pollution events originating from different directions.

[27] **Acknowledgments.** We thank all EMAC developers and modelers, especially S. Burrows, T. Butler, B. Steil, and J. Steinkamp and our MEGAPOLI partners for fruitful discussions. We acknowledge the International Max Planck Research School on Atmospheric Chemistry and Physics for financial support and the Rechenzentrum Garching, RZG, for the computing time to conduct the simulations. We appreciate the thoughtful comments on the manuscript of two anonymous referees and the editor.

[28] The Editor thanks two anonymous reviewers for their assistance in evaluating this paper.

References

- Baklanov, A., M. G. Lawrence, and S. Pandis (Eds.) (2009), MEGAPOLI—Description of work, *Rep. FP7-ENV-2007.1.1.2.1*, MEGAPOLI Proj., Copenhagen.
- Betzer, P. R., et al. (1988), Long-range transport of giant mineral aerosol particles, *Nature*, 336(6199), 568–571, doi:10.1038/336568a0.
- Burrows, S. M., et al. (2009), Bacteria in the global atmosphere—Part 2: Modeling of emissions and transport between different ecosystems, *Atmos. Chem. Phys.*, 9, 9281–9297.
- Butler, T. M., and M. G. Lawrence (2009), The influence of megacities on global atmospheric chemistry: A modelling study, *Environ. Chem.*, 6(3), 219–225.
- Dee, D. P., et al. (2011), The ERA-INTERIM reanalysis: Configuration and performance of the data assimilation system, *Q. J. R. Meteorol. Soc.*, 137(656), 553–597, doi:10.1002/qj.828.
- Emmons, L. K., et al. (2010), Impact of Mexico City emissions on regional air quality from MOZART-4 simulations, *Atmos. Chem. Phys.*, 10, 6195–6212, doi:10.5194/acp-10-6195-2010.
- Guttikunda, S. K., et al. (2003), The contribution of megacities to regional sulfur pollution in Asia, *Atmos. Environ.*, 37(1), 11–22, doi:10.1016/S1352-2310(02)00821-X.
- Jaffe, D., et al. (1999), Transport of Asian air pollution to North America, *Geophys. Res. Lett.*, 26(6), 711–714, doi:10.1029/1999GL900100.
- Jöckel, P., et al. (2005), Technical note: The Modular Earth Submodel System (MESSy)—A new approach towards Earth system modeling, *Atmos. Chem. Phys.*, 5(2), 433–444.

- Jöckel, P., et al. (2006), The atmospheric chemistry general circulation model ECHAM5/MESSy1: Consistent simulation of ozone from the surface to the mesosphere, *Atmos. Chem. Phys.*, 6(12), 5067–5104.
- Kerkweg, A., et al. (2006), Technical note: An implementation of the dry removal processes dry DEPosition and SEDimentation in the Modular Earth Submodel System (MESSy), *Atmos. Chem. Phys.*, 6(12), 4617–4632.
- Lawrence, M. G., et al. (2007), Regional pollution potentials of megacities and other major population centers, *Atmos. Chem. Phys.*, 7(14), 3969–3987.
- Lelieveld, J., et al. (2011), Global risk of radioactive fallout after nuclear reactor accident, *Atmos. Chem. Phys. Discuss.*, 11, 31,207–31,230.
- Lin, S., and R. B. Rood (1996), Multidimensional flux-form semi-Lagrangian transport schemes, *Mon. Weather Rev.*, 124(9), 2046–2070, doi:10.1175/1520-0493(1996)124<2046:MFFSLT>2.0.CO;2.
- Liu, J., et al. (2009), Evaluating inter-continental transport of fine aerosols: (1) Methodology, global aerosol distribution and optical depth, *Atmos. Environ.*, 43(28), 4327–4338, doi:10.1016/j.atmosenv.2009.03.054.
- Peel, M. C., et al. (2007), Updated world map of the Köppen-Geiger climate classification, *Hydrol. Earth Syst. Sci.*, 11(5), 1633–1644, doi:10.5194/hess-11-1633-2007.
- Pöschl, U. (2005), Atmospheric aerosols: Composition, transformation, climate and health effects, *Angew. Chem. Int. Ed.*, 44(46), 7520–7540, doi:10.1002/anie.200501122.
- Pozzer, A., et al. (2009), The influence of the vertical distribution of emissions on tropospheric chemistry, *Atmos. Chem. Phys.*, 9(24), 9417–9432, doi:10.5194/acp-9-9417-2009.
- Pringle, K. J., et al. (2010), Global distribution of the effective aerosol hygroscopicity parameter for CCN activation, *Atmos. Chem. Phys.*, 10(12), 5241–5255, doi:10.5194/acp-10-5241-2010.
- Roeckner, E., et al. (2006), Sensitivity of simulated climate to horizontal and vertical resolution in the ECHAM5 atmosphere model, *J. Clim.*, 19(16), 3771–3791, doi:10.1175/JCLI3824.1.
- Stohl, A., S. Eckhardt, C. Forster, P. James, and N. Spichtinger (2002), On the pathways and timescales of intercontinental air pollution transport, *J. Geophys. Res.*, 107(D23), 4684, doi:10.1029/2001JD001396.
- Streets, D. G., et al. (2007), Air quality during the 2008 Beijing Olympic Games, *Atmos. Environ.*, 41(3), 480–492, doi:10.1016/j.atmosenv.2006.08.046.
- Tiedtke, M. (1989), A comprehensive mass flux scheme for cumulus parameterization in large-scale models, *Mon. Weather Rev.*, 117(8), 1779–1800, doi:10.1175/1520-0493(1989)117<1779:ACMFSF>2.0.CO;2.
- Tost, H., et al. (2006), Technical note: A new comprehensive SCAVenging submodel for global atmospheric chemistry modelling, *Atmos. Chem. Phys.*, 6(3), 565–574.
- Tost, H., et al. (2007), Global cloud and precipitation chemistry and wet deposition: Tropospheric model simulations with ECHAM5/MESSy1, *Atmos. Chem. Phys.*, 7(10), 2733–2757.
- Tost, H., et al. (2010), Uncertainties in atmospheric chemistry modelling due to convection parameterisations and subsequent scavenging, *Atmos. Chem. Phys.*, 10(4), 1931–1951, doi:10.5194/acp-10-1931-2010.
- Wagstrom, K. M., and S. N. Pandis (2010), Source-receptor relationships for fine particulate matter concentrations in the eastern United States, *Atmos. Environ.*, 45(2), 347–356, doi:10.1016/j.atmosenv.2010.10.019.
- Wang, T., et al. (2010), Air quality during the 2008 Beijing Olympics: Secondary pollutants and regional impact, *Atmos. Chem. Phys.*, 10(16), 7603–7615.
- Wild, O., and H. Akimoto (2001), Intercontinental transport of ozone and its precursors in a three-dimensional global CTM, *J. Geophys. Res.*, 106(D21), 27,729–27,744, doi:10.1029/2000JD000123.

S. Borrmann and D. Kunkel, Max Planck Institute for Chemistry, PO Box 3620, Mainz D-55099, Germany. (daniel.kunkel@mpic.de)

P. Jöckel, Deutsches Zentrum für Luft und Raumfahrt, Institut für Physik der Atmosphäre, Muenchner Str. 20, Oberpfaffenhofen, Wessling D-82234, Germany.

A. Kerkweg and H. Tost, Institute for Atmospheric Physics, Johannes Gutenberg University Mainz, Mainz D-55099, Germany.

M. G. Lawrence, Institute for Advanced Sustainability Studies, Berliner Str. 130, Potsdam D-14467, Germany.